Achieving 1.2 fm/Hz$^{1/2}$ Displacement Sensitivity with Laser Interferometry in Two-Dimensional Nanomechanical Resonators: Pathways towards Quantum-Noise-Limited Measurement at Room Temperature

Jiankai Zhu[1†], Luming Wang[1†], Jiaqi Wu[1†], Yachun Liang[1], Fei Xiao[1], Bo Xu[1], Zejuan Zhang[1], Xiulian Fan[2], Yu Zhou[2*], Juan Xia[1*], and Zenghui Wang[1,3*]

[1]*Institute of Fundamental and Frontier Sciences, University of Electronic Science and Technology of China, Chengdu 610054, China*

[2]*School of Physics and Electronics, Hunan Key Laboratory of Nanophotonics and Devices, Central South University, Changsha 410083, China*

[3]*State Key Laboratory of Electronic Thin Films and Integrated Devices, University of Electronic Science and Technology of China, Chengdu 610054, China*

(Received 28 January 2022; accepted manuscript online 16 February 2023)

Laser interferometry is an important technique for ultrasensitive detection of motion and displacement. We push the limit of laser interferometry through noise optimization and device engineering. The contribution of noises other than shot noise is reduced from 92.6% to 62.4%, demonstrating the possibility towards shot-noise-limited measurement. Using noise thermometry, we quantify the laser heating effect and determine the range of laser power values for room-temperature measurements. With detailed analysis and optimization of signal transduction, we achieve 1.2 fm/Hz$^{1/2}$ displacement measurement sensitivity at room temperature in two-dimensional (2D) $CaNb_2O_6$ nanomechanical resonators, the best value reported to date among all resonators based on 2D materials. Our work demonstrates a possible pathway towards quantum-noise-limited measurement at room temperature.

DOI: 10.1088/0256-307X/40/3/038102

Interference of light is a ubiquitous physical process that encompasses both fundamental and technological importance.[1] In particular, laser interferometry has been exploited in ultrasensitive detection of displacement or motion, accomplishing some of the most well-known ultrasensitive measurements in the history of science, which dates back as early as the Michelson–Morley experiments searching for the presence of ether,[2] or as recently as the observation of gravitational wave.[3] With its superb sensitivity, it has been used from ultralarge scale experimental setups such as the kilometer-sized LIGO interferometer,[4–6] all the way to measuring ultrasmall devices such as micron- and nanometer-sized mechanical resonators.[7]

Among the many objects measured using laser interferometry, micro- and nano-mechanical resonators are particularly interesting as they constitute some of the smallest manmade mechanical structures,[8] and have been widely used in applications such as sensing,[9] computation,[10] signal processing,[11] as well as fundamental research such as exploring the boundary between the classic physics and quantum mechanics.[12–14] In these resonators there exists an intrinsic "mechanical noise": the Brownian-motion-dictated thermomechanical resonance, which represents an important limit of device motion, and sets the lower boundary of signal transduction in these mechanical structures. For typical devices, such mechanical noise is on the order of 10^1–10^2 fm/Hz$^{1/2}$; as a comparison, the Bohr radius (of a hydrogen atom) is 5.3×10^4 fm.[15] Therefore, resolving thermomechanical resonance from the measurement noise background has been an important challenge in such studies, which requires researchers to optimize the signal transduction process so that the noise floor of the measurement, i.e., sensitivity, is below (or at least close to) the thermomechanical resonance noise level.

To date, laser interferometry has been successfully used in resolving the thermomechanical resonance in many micro- and nano-mechanical resonators, including those based on two-dimensional (2D) materials and their heterostructures,[9,16] which represent some of the thinnest manmade vibrational structures: the motional part interacting with the laser can be as thin as just one individual atomic layer.[17–19] While laser interferometry has been highly successful in resolving the ultrafine motion in 2D resonators, there are still limits to its sensitivity, with shot noise being an important and fundamental one.[20]

Shot noise is a form of quantum noise[21] that originates from the quantized nature of photon, which reaches the photodetector in a discrete way with a finite level of uncertainty. Such statistical fluctuation gives rise to the shot noise, which is intrinsic to measurements of light power. While many other noises in the measurement can be minimized through optimized design and engineering, shot noise is a fundamental process and only depends on laser power, and could only be mitigated using highly

†These authors contributed equally to this work.
*Corresponding authors. Email: yu.zhou@csu.edu.cn; juanxia@uestc.edu.cn; zenghui.wang@uestc.edu.cn
© 2023 Chinese Physical Society and IOP Publishing Ltd

complicated designs such as the exotic quantum state of squeezed coherent state.[22–24] Therefore, in a measurement when all other noise sources have been minimized and shot noise dominates, it is said to be shot-noise-limited or quantum-noise-limited.[25,26] To date, such effort in pushing the limit of measurement sensitivity has not yet been reported for 2D resonators.

In this Letter, we report experimental efforts towards shot-noise-limited measurement, using laser interferometry for the detection of thermomechanical motion in nanomechanical resonators based on 2D $CaNb_2O_6$. Through detailed characterization and analysis of the noise processes, we significantly reduce the contribution of other noise sources from 92.6% to 62.4% by adjusting laser power, demonstrating potential pathways towards shot-noise-limited measurements. Via optimizing the signal transduction in measurements, we achieve a displacement sensitivity of 1.2 fm/Hz$^{1/2}$ at 304 K. In comparison, the diameter of an individual hydrogen atomic nucleus is 1.70 fm.[27,28] This represents the best value reported to date in room temperature interferometric measurements of 2D resonators. Our work demonstrates an effective and systematic approach for improving signal transduction and measurement sensitivity in interferometric motion detection.

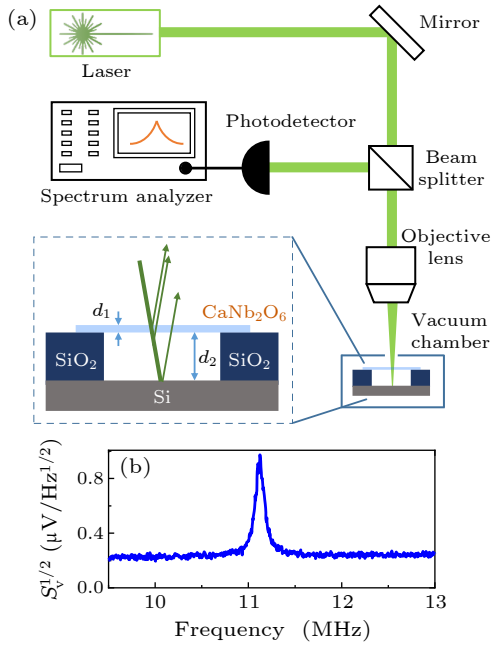

Fig. 1. Thermomechanical motion measurement. (a) Custom-built interferometry system. Inset shows the device structure and a schematic illustration of the interferometry process. (b) Example of measured noise spectrum from a device.

Figure 1(a) shows the signal transduction process with laser interferometry. The nanomechanical devices assume drumhead structures with calcium niobate ($CaNb_2O_6$) diaphragms fully covering microtrenches with different diameters. $CaNb_2O_6$, naturally occurring in the mineral fersmite, has recently attracted increasing attention as a type of 2D perovskite.[29–31] It has a large bandgap (3.5 eV), and has potential applications in UV photodetection.[32,33] The devices are fabricated using a dry transfer technique,[34,35] and are characterized using AFM and optical spectroscopy to verify the structural and material integrity (Fig. S1 in the Supplementary Material). As illustrated in the inset of Fig. 1(a), the incident laser reflects at all the interfaces (from top to bottom: vacuum/$CaNb_2O_6$, $CaNb_2O_6$/vacuum, vacuum/Si), and the total reflectance of the device structure can be calculated using a Fresnel-law optical model,[36,37] which accounts for the interference from the multi-reflection process. The reflectance can be modulated by the change of vacuum gap depth d_2, thus transducing the device motion.

The ultrasensitive motion detection system is shown in Fig. 1(a). Each device is mounted in a room-temperature vacuum chamber ($\sim 10^{-6}$ Torr). We focus the beam from a 532 nm laser (MSL-FN-532-50 mW) onto the suspended part of the device using a long-working-distance objective lens, and collect the reflected light with a photodetector [specifications provided below in calculations using Eqs. (1) and (2)]. We then measure the noise power spectrum in the reflected light power using a spectrum analyzer, with a typical result shown in Fig. 1(b). The noise spectrum shows a sharp peak on top of a slowly varying background. The peak corresponds to a mechanical resonance mode of the device excited by thermal noise (Brownian resonance). For all devices, we check their noise spectrum over a large frequency range to ensure that the fundamental mode resonance is measured, unless when intentionally studying the higher modes.

To achieve ultrasensitive measurements, one needs to optimize the signal-to-noise ratio (SNR). We therefore first analyze all the noise sources in such measurements. The total voltage domain noise spectral density $S_v^{1/2}$ includes contributions from (1) device thermomechanical noise $S_{v,th}^{1/2}$ (note that, while physically it is a noise process, in our measurements it is the "signal"; the following terms (2)–(4) constitute the system noise floor $S_{v,sys}^{1/2}$), (2) noise from the spectrum analyzer $S_{v,SA}^{1/2}$, (3) electronic noise from the photodetector (PD) $S_{v,PD}^{1/2}$, and (4) laser noise, which further includes shot noise $S_{v,shot}^{1/2}$ and excessive laser noise $S_{v,laser}^{1/2}$. A better SNR means that $S_{v,NEMS}^{1/2}$ constitutes a larger fraction of the total noise $S_{v,total}^{1/2} = \left(\sum_j S_{v,j}\right)^{1/2}$ at the resonance frequency, which further translates to better measurement sensitivity.

Contribution of each noise source can be quantified by taking noise spectrum under different configurations, with the result shown in Fig. 2 [note that, while data with the same set of five colors are included in all panels, they are most distinguishable in Fig. 2(c)]. First, with nothing connected, we measure a very low noise from the spectrum analyzer (orange curve). We then connect the photodetector to the spectrum analyzer while blocking all lights, and measure an increased noise level (blue curve) due to the electronic noise of the photodetector. As laser is allowed to reach the photodetector, the noise level further increases (magenta curve). Finally, as the laser spot moves onto the device, thermomechanical resonances appear as sharp peaks in the noise spectrum (red curve).

Here we estimate the shot noise to further understand the laser noise. The electric current domain spectral density is [38]

$$S_{\mathrm{i}}^{1/2} = (2eP_{\mathrm{in}}\Re_{\mathrm{PD}})^{1/2}, \tag{1}$$

where e is electron charge, P_{in} is the laser power incident on the photodetector, and $\Re_{\mathrm{PD}}$ is the laser-power-to-current responsivity of the photodiode. In the measurements shown in Fig. 2(c), $P_{\mathrm{in}} = 2.22\,\mathrm{mW}$ and $\Re_{\mathrm{PD}} = 0.33\,\mathrm{A/W}$ (obtained from the datasheet of the PD for 532 nm illumination), thus the shot noise is (note that for 1 Coulomb of charge, $1\,\mathrm{C} = 1\,\mathrm{A/Hz}$):

$$\begin{aligned} S_{\mathrm{i}}^{1/2} &= [2 \times 1.6 \times 10^{-19}\,\mathrm{C} \times 2.22 \times 10^{-3}\,\mathrm{W} \\ &\quad \times 0.33\,\mathrm{A \cdot W^{-1}}]^{1/2} \\ &= 1.53 \times 10^{-11}\,\mathrm{A \cdot Hz^{-1/2}}. \end{aligned} \tag{2}$$

This value is then converted into the voltage domain with the transimpedance gain G (40 V/mA for the PD is observed in our measurements; the value obtained from the datasheet of the PD is constant within its operation bandwidth):

$$\begin{aligned} S_{\mathrm{v}}^{1/2} &= S_{\mathrm{i}}^{1/2} \times G = 1.53 \times 10^{-11}\,\mathrm{A \cdot Hz^{-1/2}} \times 40000\,\mathrm{V \cdot A^{-1}} \\ &= 6.12 \times 10^{-7}\,\mathrm{V \cdot Hz^{-1/2}}, \end{aligned} \tag{3}$$

The resulting voltage noise is equally divided between the 50 Ω output impedance of the photodetector and the 50 Ω input impedance of the spectrum analyzer, resulting in a net contribution of $3.06 \times 10^{-7}\,\mathrm{V/Hz^{1/2}}$ to the measurement, which is illustrated by the green curves in Fig. 2.

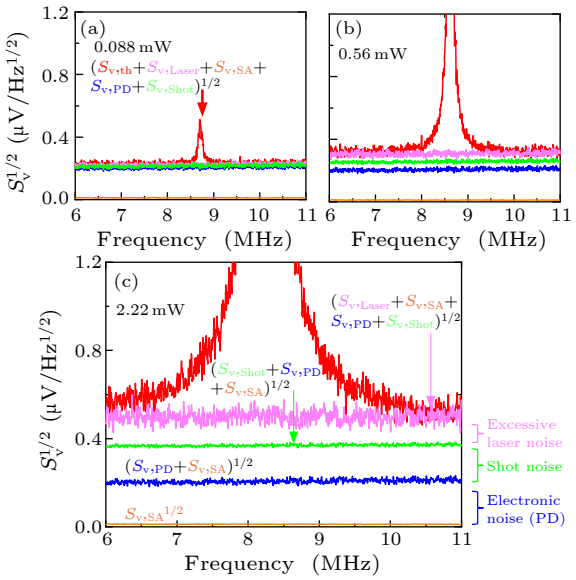

Fig. 2. Noise analysis in interferometric measurements. Data are shown for on-detector laser power of (a) 0.088 mW, (b) 0.56 mW, and (c) 2.22 mW. All panels show the data measured with (1) only spectrum analyzer (orange), (2) spectrum analyzer + PD (no light) (blue), (3) spectrum analyzer + PD + shot noise (calculation) (green), (4) spectrum analyzer + PD + laser noise (measurement) (magenta), and (5) spectrum analyzer + PD + laser + device motion (thermomechanical noise) (red).

At low laser power [0.088 mW, Fig. 2(a)], we observe that the most important contribution comes from electronic noise from the photodetector ($S_{\mathrm{v,PD}}^{1/2}$). To move towards the shot noise limit in our measurements, we minimize the contribution from the photodetector noise ($S_{\mathrm{v,PD}}^{1/2}$) by increasing laser power from 0.088 mW [Fig. 2(a)] all the way to 2.22 mW [Fig. 2(c)], while performing noise analysis of the same device. One can clearly see that as the laser power increases, in $S_{\mathrm{v,sys}}^{1/2}$ the relative contribution of the photodetector is significantly reduced (from 84.43% to 17.09% of the total noise), and the contribution of shot noise gradually increases in the noise process from 7.4% to 37.6% at the device resonance frequency (8.263 MHz), i.e., reducing the contribution of other noise sources from 92.6% to 62.4% through increasing laser power. This shows a possible pathway towards shot-noise-limited measurements.

It is important to note that, while increasing laser power leads to greater shot noise, it increases the resonance signal even further. This is because the origin of shot noise is a Poisson process whose average amplitude is proportional to the square root of laser power. In contrast, the measured motional signal scales linearly with the laser power. Consequently, the shot-noise-limited SNR increases with the square root of laser power (Fig. S2). Further, other noises such as those from the spectrum analyzer and photodetector do not increase with laser power [Fig. 2(a) vs Fig. 2(c)]. Therefore, increasing the laser power effectively improves the SNR of the measurement through both the mechanisms, and leads to better measurement sensitivity in the displacement domain.

Next, we extract the displacement-domain information from the voltage-domain measurements, in order to obtain details of the device motion and the measurement sensitivity. To correlate the measured signal in the voltage domain to the mechanical displacement of the device, we analyze the data using the following expression, which describes a resonator's thermomechanical noise spectral density as a function of angular frequency ω in the displacement domain: [39]

$$S_{\mathrm{x,th}}^{1/2}(\omega) = \left[\frac{4\omega_0 k_{\mathrm{B}} T}{Q M_{\mathrm{eff}}} \cdot \frac{1}{(\omega_0^2 - \omega^2)^2 + (\omega_0\omega/Q)^2}\right]^{1/2}. \tag{4}$$

Here, k_{B}, T, ω_0, Q, and M_{eff} are the Boltzmann's constant, absolute temperature, angular resonance frequency of the particular resonance mode, quality factor, and the effective mass of the device, respectively. At the resonance frequency, the expression becomes

$$S_{\mathrm{x,th}}^{1/2}(\omega_0) = \sqrt{\frac{4k_{\mathrm{B}}TQ}{\omega_0^3 M_{\mathrm{eff}}}}. \tag{5}$$

For a device whose data is shown in Fig. 3, using its measured resonance frequency ($f_0 = 11.13\,\mathrm{MHz}$), quality factor ($Q = 140$), device dimensions (thickness $d_1 = 69.1\,\mathrm{nm}$, diameter $d = 7\,\mu\mathrm{m}$), material density ($\rho_{3\mathrm{D}} = 4800\,\mathrm{kg/m^3}$), [40] mode shape ($M_{\mathrm{eff}}/M = 0.1828$ for the fundamental mode, [41] where M is the resonator mass), and device temperature (here we first assume that the device works at 300 K, which will be experimentally determined later), using Eq. (5) we determine its on-resonance

thermomechanical noise spectral density (in the displacement domain) to be $S_{\mathrm{x,th}}^{1/2} = 53.85\,\mathrm{fm/Hz^{1/2}}$.

In such noise measurements, the total noise power spectral density (PSD) is equal to the sum of PSDs from individual noise processes, based on the assumption that all noise processes are uncorrelated. One can therefore write $S_{\mathrm{v,total}}^{1/2} = (S_{\mathrm{v,th}} + S_{\mathrm{v,sys}})^{1/2}$. Again, $S_{\mathrm{v,th}}^{1/2}$ is the thermomechanical motion noise of the device expressed in the voltage domain, which is related to the displacement domain noise through the 'displacement-to-voltage' responsivity $\Re \equiv S_{\mathrm{v,th}}^{1/2}/S_{\mathrm{x,th}}^{1/2}$. $S_{\mathrm{v,sys}}^{1/2}$ is the electronic noise floor of the entire measurement system, which determines the off-resonance background ($S_{\mathrm{v,total}}^{1/2} \approx S_{\mathrm{v,sys}}^{1/2}$ at frequencies far away from the resonance). $S_{\mathrm{v,sys}}^{1/2}$ includes contributions from all the noise sources (e.g., spectrum analyzer, photodetector, laser) other than the thermomechanical motion of the device, as analyzed in Fig. 2.

We therefore fit the measured noise spectrum to the expression

$$S_{\mathrm{v,total}}^{1/2} = (\Re^2 \times S_{\mathrm{x,th}} + S_{\mathrm{v,sys}})^{1/2} = \sqrt{\Re^2\Big(\frac{4\omega_0 k_{\mathrm{B}} T}{Q M_{\mathrm{eff}}} \cdot \frac{1}{(\omega_0^2-\omega^2)^2 + (\omega_0\omega/Q)^2}\Big) + S_{\mathrm{v,sys}}}, \tag{6}$$

in which we use the relationship $S_{\mathrm{v,th}}^{1/2} = \Re \times S_{\mathrm{x,th}}^{1/2}$. We then extract $S_{\mathrm{v,sys}}^{1/2}$, Q, and $\Re$ (again, assuming $T = 300\,\mathrm{K}$) from the fitting using Eq. (6). During the fitting we treat $S_{\mathrm{v,sys}}^{1/2}$ as a frequency-dependent function, whose numerical values are obtained from the experimental measurements (Fig. S3).

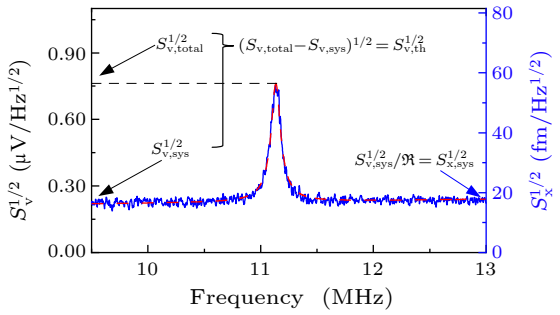

Fig. 3. Calculation of the displacement-to-voltage responsivity from measured noise spectrum in a device (69.1 nm thick, with on-device laser power 0.56 mW), assuming a device temperature of 300 K, with annotations indicating how various quantities can be read off from the figure and are related to each other. The dashed line shows fitting using Eq. (6).

The dashed line in Fig. 3 shows an example of such fitting. Measured voltage domain noise spectrum $S_{\mathrm{v,total}}^{1/2}$ is plotted against the left y-axis, while displacement domain noise spectral density, converted through the relationship $S_x^{1/2} = S_v^{1/2}/\Re$, is plotted against the right y-axis. From this we can obtain the displacement sensitivity $S_{\mathrm{x,sys}}^{1/2} = S_{\mathrm{v,sys}}^{1/2}/\Re$ for the measurement, which scales with the voltage domain noise floor of the entire measurement system. For the specific measurement in Fig. 3, at the device resonance frequency (11.13 MHz) the displacement sensitivity in our measurement system is $S_{\mathrm{x,sys}}^{1/2} = 16.95\,\mathrm{fm/Hz^{1/2}}$.

The above analysis assumes that the device is at room temperature (300 K), which is important for fair comparison of measurement sensitivity. As the devices are illuminated by laser, possible laser heating effect can be present. However, experimentally determining the temperature of a suspended 2D flake is particularly challenging, given the small dimensions of our devices and the absence of electrical contacts, which preclude the application of conventional thermometry techniques. Here we use noise thermometry to measure the device temperature, which exploits the intrinsic physical process of thermomechanical vibration, and use the device itself as a thermometer.[39,42–44]

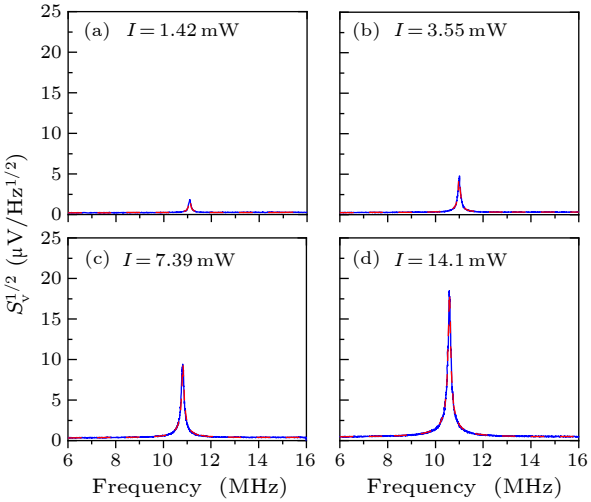

Fig. 4. Dependence of measured noise spectrum on on-device laser power for the same device (69.1 nm thick) in Fig. 3. Results are shown for on-device laser power values of (a) 1.42 mW, (b) 3.55 mW, (c) 7.39 mW, and (d) 14.1 mW. Dashed lines show fittings using Eq. (6).

This is carried out by analyzing the noise spectrum of the device's thermomechanical motion at a series of laser power levels (Figs. 4 and S4). By integrating Eq. (4) over frequency and rearranging the terms, the device temperature can be expressed using its thermomechanical motion amplitude:

$$T = \frac{k_{\mathrm{eff}}}{2\pi k_{\mathrm{B}}} \int_0^\infty S_{\mathrm{x,th}}(\omega) d\omega. \tag{7}$$

Here, $k_{\mathrm{eff}} = \omega_0^2 M_{\mathrm{eff}}$ is the effective spring constant of the resonator. We then use the relationship $S_{\mathrm{v,th}}^{1/2} = \Re \times S_{\mathrm{x,th}}^{1/2}$ to express T using the measured voltage domain spectrum density:

$$T = \frac{k_{\mathrm{eff}}}{2\pi k_{\mathrm{B}}} \int_0^\infty \Big(\frac{S_{\mathrm{v,th}}^{1/2}(\omega)}{\Re}\Big)^2 d\omega. \tag{8}$$

As the displacement-to-voltage responsivity $\Re$ linearly depends on the incident (on-device) laser power I, one can reach

$$T = C\frac{k_{\mathrm{eff}}}{2\pi k_{\mathrm{B}}} \int_0^\infty \Big(\frac{S_{\mathrm{v,th}}^{1/2}(\omega)}{I}\Big)^2 d\omega, \tag{9}$$

where C is a constant independent of incident laser power levels. The form of Eq. (9) suggests that as long as the

measured noise power (obtained through fitting and integrated over all frequencies) remains proportional to I^2, the device temperature is unchanged. In this case, one can conclude that there is negligible laser heating effect, and the device temperature should be equilibrized with that of the thermal bath, which equals room temperature in our experiments.

We therefore integrate thermomechanical noise measured under different on-device laser intensities (Fig. 4 and S4) over all frequencies for each device, and estimate the change in device temperature using Eq. (9), with the results shown in Fig. 5. We find that for all devices, the temperature remains roughly constant (and therefore room temperature) for small on-device laser powers, and only starts to clearly increase for on-device laser powers beyond 3.55 mW. This is due to the very large bandgap of $CaNb_2O_6$ (3.46 eV),[45] which translates to minimal laser heating.

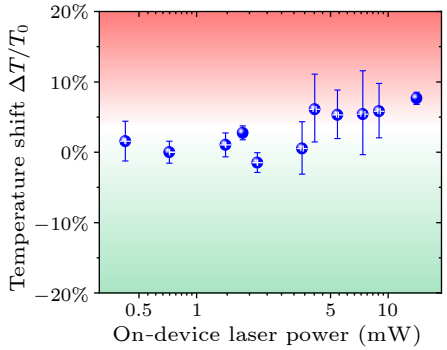

Fig. 5. Measured device temperature under different levels of incident (on-device) laser power, for the same device (69.1 nm thick) in Fig. 3. Error bars are calculated from the uncertainty in laser power measurements and fitting uncertainty.

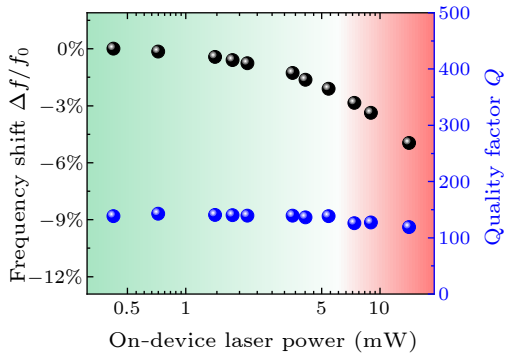

Fig. 6. Measured device resonance frequency (black) and quality factor (blue) under different levels of incident (on-device) laser power for the same device (69.1 nm thick) in Fig. 3.

In addition to noise thermometry analysis, we also plot the resonance frequency f and quality factors Q of the same device in Fig. 6. We can see that these values remain roughly unchanged when the device is at room temperature. To quantitatively correlate the resonance frequency to device temperature,[46] we measure the temperature coefficient of frequency (TCf) for these devices (Fig. 7). With these measurements, we can clearly identify the actual temperature of all measurements, and use them for sensitivity analysis.

The choice of $CaNb_2O_6$ as the resonator material is also critical for achieving superb sensitivity. Not only does its large bandgap allow the use of relatively large laser power, its higher index of refraction (2.28 at 532 nm,[31] compared with 2.2 for h-BN[47]) also leads to improved signal transduction. Specifically, the 'displacement-to-reflectance' responsivity is directly related to the index of refraction.[36,37] Therefore, interferometric motion detection in $CaNb_2O_6$ resonators can be more efficient than resonators based on h-BN,[47,48] the archetypical 2D insulator.

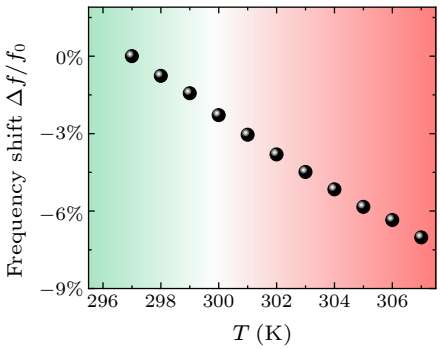

Fig. 7. TCf measurement for the same device (69.1 nm thick) in Fig. 3. The resonance measurement is performed in a cryostat, with an on-device laser power of 0.51 mW, which does not heat the device. The device temperature is controlled by a temperature controller that controls a resistive heater near the end of the cooling head of the cryostat (no cooling power during the experiment), and read off from a silicon diode temperature sensor mounted near the heater. Both the heater and temperature sensor are close (within a few mm) to and have good thermal contact (using an all-metal sample holder) with the resonator device chip, which is mounted at the end of the cooling head.

To optimize the signal transduction process, we calculate the displacement-to-reflectance responsivity for $CaNb_2O_6$ resonators. Our findings (Fig. S8) show that for devices with 290 nm vacuum gap between the $CaNb_2O_6$ resonator and the silicon substrate, under 532 nm illumination the optimal device thickness is $\sim$ 50 nm, which gives the highest responsivity of 1.53%/nm. We therefore focus on measuring devices in this thickness range. We also confirm that for $CaNb_2O_6$ resonators, 532 nm laser (we use) leads to greater maximum responsivity than 633 nm laser, which is commonly used in measurements of other 2D resonators[18,34,49] and could further translate to better SNR and sensitivity in measurements (Fig. S9).

We therefore focus on using 532 nm laser for achieving the best measurement sensitivity. Figure 8 shows the measured result of the device with thickness of 69.1 nm, in which we achieve record-breaking measurement sensitivities of $S_{x,sys}^{1/2} = 3.55\,\mathrm{fm/Hz^{1/2}}$ at 298 K, and $1.35\,\mathrm{fm/Hz^{1/2}}$ at 304 K. Figure 9 shows the measured result of another device with thickness of 44.8 nm (full data in Figs. S5–S7),

in which we achieve even better measurement sensitivities of $S_{x,sys}^{1/2} = 3.37\,\mathrm{fm/Hz^{1/2}}$ at 298 K, and $1.24\,\mathrm{fm/Hz^{1/2}}$ at 304 K. These values are at least one order of magnitude better than most reported values for interferometric measurements of 2D resonators, and also surpass those reported for resonators based on other materials such as Si,[40,50–52] SiN,[53–55] and SiC.[38] Such excellent sensitivity allows us to detect up to 24 modes of Brownian resonance, and even better, to spatially map out the mode shape,[38,49,56,57] for all these thermomechanical modes (Figs. S10 and S11). This again demonstrates the powerfulness of our ultrasensitive interferometric measurement setup in resolving ultrafine mechanical motion in nanoscale devices.

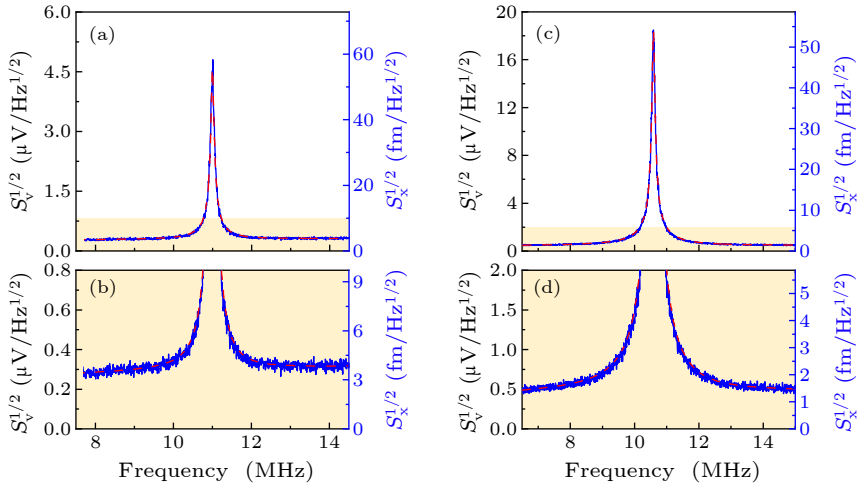

Fig. 8. Measurements of thermomechanical motion and displacement sensitivity in a $CaNb_2O_6$ nanomechanical resonator (69.1 nm thick). (a) Measured noise spectrum with on-device laser power of 3.55 mW, with a measured device temperature of 298 K. (b) Enlargement of the colored area in (a), showing the measurement noise floor in both voltage and displacement domains, and a sensitivity of $3.55\,\mathrm{fm/Hz^{1/2}}$. (c) Measured noise spectrum with on-device laser power of 14.1 mW, with a measured device temperature of 304 K. (d) Enlargement of the colored area in (c), showing the measurement noise floor in both voltage and displacement domains, and a sensitivity of $1.35\,\mathrm{fm/Hz^{1/2}}$. Dashed lines show fittings using Eq. (6).

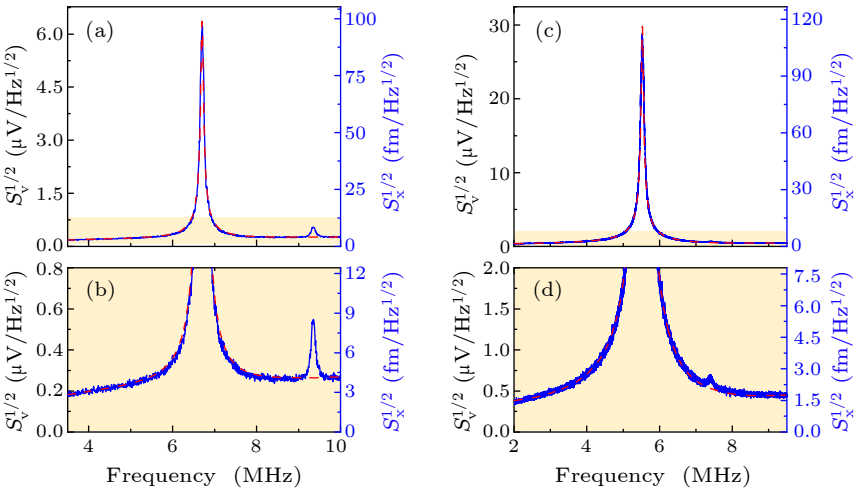

Fig. 9. Measurements of thermomechanical motion and displacement sensitivity in a $CaNb_2O_6$ nanomechanical resonator (44.77 nm thick, full data in Figs. S5–S7). (a) Measured noise spectrum with on-device laser power of 3.55 mW, with a measured device temperature of 298 K. (b) Enlargement of the colored area in (a), showing the measurement noise floor in both voltage and displacement domains, and a sensitivity of $3.37\,\mathrm{fm/Hz^{1/2}}$. (c) Measured noise spectrum with on-device laser power of 14.1 mW, with a measured device temperature of 304 K. (d) Enlargement of the colored area in (c), showing the measurement noise floor in both voltage and displacement domains, and a sensitivity of $1.24\,\mathrm{fm/Hz^{1/2}}$. Dashed lines show fittings using Eq. (6).

Table 1 offers a comparison of displacement sensitivity in measurements of micro/nano resonators, with resonator material, measurement technique, and measurement temperature shown. Not only do our results surpass all reported values measured with optical interferometry, but our measurement sensitivity is also on par with, or even better than, those achieved using more complicated device designs such as single electron transistor, supercon-

ducting microwave cavity, and superconducting quantum interference devices (SQUIDs), and under millikelvin temperatures. It is important to note that several sensitivity values are reported by assuming absence of laser heating for large-bandgap 2D materials.[47,58] In our work, we perform noise thermometry and TCf measurements, and find that such heating could still be present even for 2D resonators based on large-bandgap materials, possibly due to heat absorption in the silicon substrate. Consequently, we determine device temperature at each laser power, and the room temperature sensitivity values reported in our work are backed up by careful temperature calibration.

Table 1. Comparison of measurement sensitivity using different techniques.

Work	Resonator Material	Measurement Technique	Measurement Temperature	Displacement Sensitivity ($\mathrm{fm/Hz^{1/2}}$)
Ref. [53]	SiN	Single electron transistor	35–100 mK	3.8
Ref. [59]	Si	SQUID	20 mK	10
Ref. [60]	Graphene	Superconducting microwave cavity	96 mK	17
Ref. [61]	Si	Optomechanical detection	300 K (uncalibrated)	7
Ref. [62]	Si	Near-field optical transduction	300 K (uncalibrated)	150
Ref. [63]	Si	Evanescent light scattering	300 K (uncalibrated)	260
Ref. [44]	Si	Optical interferometry	4.2 K	$\sim$1000
Ref. [30]	SiC	Optical interferometry	300 K (uncalibrated)	7–14
Ref. [54]	SiN	Optical interferometry	300 K (uncalibrated)	75
Ref. [50]	Si	Optical interferometry	308 K	166
Ref. [55]	SiN	Optical interferometer	300 K (uncalibrated)	100
Ref. [51]	Si	Optical interferometry	300 K (uncalibrated)	300
Ref. [52]	Si	Optical interferometry	300 K (uncalibrated)	5000 [estimated from its Fig. 3(b)]
Ref. [64]	Graphene	Optical interferometry	100 K	600
Ref. [65]	Graphene	Optical interferometry	300 K (uncalibrated)	11
Ref. [49]	$Ti_3C_2T_x$	Optical interferometry	300 K (uncalibrated)	194.67
Ref. [34]	Black P	Optical interferometry	300 K (uncalibrated)	25 (estimated from its Fig. 5)
Ref. [17]	Graphene	Optical interferometry	300 K (uncalibrated)	220 [estimated from its Fig. 4(a)]
Ref. [47]	h-BN	Optical interferometry	300 K (uncalibrated)	12.9
Ref. [58]	Ga_2O_3	Optical interferometry	300 K (uncalibrated)	4–19
Ref. [66]	ReS_2	Optical interferometry	300 K (uncalibrated)	79.3
Ref. [41]	MoS_2	Optical interferometry	300 K	49.5
This work	$CaNb_2O_6$	Optical interferometry	298 K	3.4
This work	$CaNb_2O_6$	Optical interferometry	304 K	1.2

In summary, we have carried out a detailed study of the noise processes in interferometric measurement of thermomechanical resonance in 2D resonators. Through detailed noise analysis, we successfully reduce the weight of other noises in the measurement from 92.6% to 62.4% through adjusting laser power, making shot noise more dominant in the noise process. We further optimize interferometric signal transduction through engineering device dimension and material, and achieve a room-temperature displacement sensitivity of $1.2\,\mathrm{fm/Hz^{1/2}}$ at 304 K, setting a new record for 2D resonators. Our work demonstrates a potential pathway towards shot-noise-limited measurement at room temperature, or even better, resolving motional noise at temperatures lower than the room temperature. In particular, for typical monolayer 2D resonators the quantum fluctuation becomes dominant below $\sim$100 mK,[67] which is achievable with the cryogenic technology today. It would therefore be very interesting to explore the potential use of laser interferometry in resolving such quantum-fluctuation-limited motional noise in these nanomechanical devices, and even further, using such manmade structures to study the boundary and transition between quantum mechanics and classical mechanics.

Acknowledgements. This work was supported by the National Key R&D Program of China (Grant No. 2022YFB3203600), the National Natural Science Foundation of China (Grant Nos. 62150052, 62250073, U21A20459, 62004026, 61774029, 62104029, and 12104086), the Sichuan Science and Technology Program (Grant No. 2021YJ0517 and 2021JDTD0028), the Natural Science Foundation of Hunan Province (Grant No. 2021JJ40780), and the Science and Technology Innovation Program of Hunan Province "HuXiang Young Talents" (Grant No. 2021RC3021). Zenghui Wang thanks Professor Jaesung Lee for helpful discussion.

References

[1] Kipnis N 2012 *History of the Principle of Interference of Light* (Birkhäuser)
[2] Michelson A A and Morley E W 1887 *Am. J. Sci.* **3** 333
[3] Abbott B P *et al.* (LIGO Scientific Collaboration and Virgo Collaboration) 2016 *Phys. Rev. Lett.* **116** 061102
[4] Weiss R 2018 *Rev. Mod. Phys.* **90** 040501
[5] Barish B C 2018 *Rev. Mod. Phys.* **90** 040502
[6] Thorne K S 2018 *Rev. Mod. Phys.* **90** 040503
[7] Rugar D, Budakian R, Mamin H J, and Chui B W 2004 *Nature* **430** 329
[8] Bachtold A, Moser J, and Dykman M I 2022 *Rev. Mod. Phys.* **94** 045005
[9] Xu B, Zhang P C, Zhu J K, Liu Z H, Eicher A, Zheng X Q, Lee J, Dash A, More S, Wu S, Wang Y N, Jia H, Naik

A, Bachtold A, Yang R, Feng P X L, and Wang Z H 2022 *ACS Nano* **16** 15545
[10] Wang Z H, Fang J W, Zhang P C, and Yang R 2021 *Sci. Chin. Inform. Sci.* **64** 206401
[11] Nguyen C T C 2007 *IEEE Trans. Ultrason. Ferr.* **54** 251
[12] O'Connell A D, Hofheinz M, Ansmann M, Bialczak R C, Lenander M, Lucero E, Neeley M, Sank D, Wang H, Weides M, Wenner J, Martinis J M, and Cleland A N 2010 *Nature* **464** 697
[13] Kotler S, Peterson G A, Shojaee E, Lecocq F, Cicak K, Kwiatkowski A, Geller S, Glancy S, Knill E, Simmonds R W, Aumentado J, and Teufel J D 2021 *Science* **372** 622
[14] Mercier de Lépinay L, Ockeloen-Korppi C F, Woolley M J, and Sillanpää M A 2021 *Science* **372** 625
[15] 2018 *CODATA Value: Bohr Radius* (The NIST Reference on Constants, Units, and Uncertainty) NIST 20 May 2019
[16] Wang Z H, Xu B, Pei S H, Zhu J K, Wen T, Jiao C Y, Li J, Zhang M D, and Xia J 2022 *Sci. Chin. Inform. Sci.* **65** 211401
[17] Bunch J S, van der Zande A M, Verbridge S S, Frank I W, Tanenbaum D M, Parpia J M, Craighead H G, and McEuen P L 2007 *Science* **315** 490
[18] Zhu J K, Xu B, Xiao F, Liang Y C, Jiao C Y, Li J, Deng Q Y, Wu S, Wen T, Pei S H, Xia J, and Wang Z H 2022 *Nano Lett.* **22** 5107
[19] Lee J, Wang Z H, He K L, Yang R, Shan J, and Feng P X L 2018 *Sci. Adv.* **4** eaao6653
[20] Verdeyen J T 1995 *Laser Electronics* 3rd edn (Prentice-Hall)
[21] Stevenson A J, Gray M B, Bachor H A, and McClelland D E 1993 *Appl. Opt.* **32** 3481
[22] Dutt A, Luke K, Manipatruni S, Gaeta A L, Nussenzveig P, and Lipson M 2015 *Phys. Rev. Apll.* **3** 044005
[23] Aasi J *et al.* 2013 *Nat. Photon.* **7** 613
[24] The LIGO Scientific Collaboration 2011 *Nat. Phys.* **7** 962
[25] Michaud-Belleau V, Deschênes J D, and Genest J 2022 *IEEE J. Quantum Electron.* **58** 6100211
[26] Saraf S, Urbanek K, Byer R L, and King P J 2005 *Opt. Lett.* **30** 1195
[27] Castelvecchi D 2019 *Nature* **575** 269
[28] Antognini A *et al.* 2013 *Science* **339** 417
[29] Cummings J P and Simonsen S H 1970 *Am. Mineral.* **55** 90
[30] Moreira R L, Teixeira N G, Andreeta M R B, Hernandes A C, and Dias A 2010 *Cryst. Growth* **10** 1569
[31] Feng G L, Li L, and Xu D P 2021 *Crystals* **11** 928
[32] Duman U, Aycibin M, and Özdemir Ö F 2021 *Phys. Status Solidi B* **258** 2100416
[33] Qin J K, Xiao H, Zhu C Y, Zhen L, and Xu C Y 2022 *Adv. Opt. Mater.* **10** 2201627
[34] Wang Z H, Jia H, Zheng X Q, Yang R, Wang Z F, Ye G J, Chen X H, Shan J, and Feng P X L 2015 *Nanoscale* **7** 877
[35] Liang Y C, Zhu J K, Xiao F, Xu B, Wen T, Wu S, Li J, Xia J, and Wang Z H 2021 *IEEE J. Electron. Devices Soc.* **9** 1269
[36] Wang Z H and Feng P X L 2016 *Sci. Rep.* **6** 28923
[37] Zhu J K, Zhang P C, Yang R, and Wang Z H 2022 *Sci. Chin. Inform. Sci.* **65** 122409
[38] Wang Z H, Lee J, and Feng P X L 2014 *Nat. Commun.* **5** 5158
[39] Cleland A N 2013 *Foundations of Nanomechanics: From Solid-State Theory to Device Applications* (Springer Science & Business Media)
[40] Ballman A A, Porto S P S, and Yariv A 1963 *J. Appl. Phys.* **34** 3155
[41] Lee J, Wang Z H, He K L, Shan J, and Feng P X L 2013 *ACS Nano* **7** 6086
[42] Bleszynski-Jayich A C, Shanks W E, and Harris J G E 2008 *Appl. Phys. Lett.* **92** 013123
[43] Montinaro M, Mehlin A, Solanki H S, Peddibhotla P, Mack S, Awschalom D D, and Poggio M 2012 *Appl. Phys. Lett.* **101** 133104
[44] Poggio M, Degen C L, Mamin H J, and Rugar D 2007 *Phys. Rev. Lett.* **99** 017201
[45] Cho I S, Bae S T, Yim D K, Kim D W, and Hong K S 2009 *J. Am. Ceram. Soc.* **92** 506
[46] Wang Z H, Yang R, and Feng P X L 2021 *Nanoscale* **13** 18089
[47] Zheng X Q, Lee J, and Feng P X L 2017 *Microsyst. Nanoeng.* **3** 17038
[48] Zheng X Q, Lee J, and Feng P X L 2015 *IEEE Transducers - 18th International Conference on Solid-State Sensors, Actuators and Microsystems (TRANSDUCERS)*, 21–25 June 2015, Anchorage, AK, USA, pp 1393–1396
[49] Xu B, Zhu J K, Xiao F, Liu N, Liang Y C, Jiao C Y, Li J, Deng Q Y, Wu S, Wen T, Pei S H, Wan H J, Xiao X, Xia J, and Wang Z H 2022 *ACS Nano* **16** 20229
[50] Hiebert W K, Vick D, Sauer V, and Freeman M R 2010 *J. Micromech. Microeng.* **20** 115038
[51] Azak N O, Shagam M Y, Karabacak D M, Ekinci K L, Kim D H, and Jang D Y 2007 *Appl. Phys. Lett.* **91** 093112
[52] Kouh T, Karabacak D, Kim D H, and Ekinci K L 2005 *Appl. Phys. Lett.* **86** 013106
[53] LaHaye M D, Buu O, Camarota B, and Schwab K C 2004 *Science* **304** 74
[54] Losby J, Burgess J A, Diao Z, Fortin D C, Hiebert W K, and Freeman M R 2012 *J. Appl. Phys.* **111** 07D305
[55] Rajauria S, Ozsun O, Lawall J, Yakhot V, and Ekinci K L 2011 *Phys. Rev. Lett.* **107** 174501
[56] Wang Z H, Jia H, Zheng X Q, Yang R, Ye G J, Chen X H, and Feng P X L 2016 *Nano Lett.* **16** 5394
[57] Wang Z H, Lee J, He K L, Shan J, and Feng P X L 2014 *Sci. Rep.* **4** 3919
[58] Zheng X Q, Lee J, Rafique S, Han L, Zorman C A, Zhao H P, and Feng P X L 2017 *ACS Appl. Mater. Interfaces* **9** 43090
[59] Etaki S, Poot M, Mahboob I, Onomitsu K, Yamaguchi H, and van der Zant H S J 2008 *Nat. Phys.* **4** 785
[60] Singh V, Bosman S J, Schneider B H, Blanter Y M, Castellanos-Gomez A, and Steele G A 2014 *Nat. Nanotechnol.* **9** 820
[61] Kim P H, Doolin C, Hauer B D, MacDonald A J, Freeman M R, Barclay P E, and Davis J P 2013 *Appl. Phys. Lett.* **102** 053102
[62] Basarir O, Bramhavar S, and Ekinci K L 2010 *Appl. Phys. Lett.* **97** 253114
[63] Basarir O, Bramhavar S, Basilio-Sanchez G, Morse T, and Ekinci K L 2010 *Opt. Lett.* **35** 1792
[64] Barton R A, Storch I R, Adiga V P, Sakakibara R, Cipriany B R, Ilic B, Wang S P, Ong P J, McEuen P L, Parpia J M, and Craighead H G 2012 *Nano Lett.* **12** 4681
[65] Davidovikj D, Slim J J, Cartamil-Bueno S J, van der Zant H S J, Steeneken P G, and Venstra W J 2016 *Nano Lett.* **16** 2768
[66] Zhu J K, Xiao F, Jiao C Y, Liang Y C, Wen T, Wu S, Zhang Z J, Lin L, Pei S H, Jia H, Ren Z M, Wei X Y, Huang W, Xia J, and Wang Z H 2023 *Small* (in press)
[67] Wang Z H and Feng P X L 2014 *Appl. Phys. Lett.* **104** 103109